New Molecular Arrays Based on a Tin(IV) Porphyrin Scaffold

A. Ashok Kumar, L. Giribabu, D. Raghunath Reddy, and Bhaskar G. Maiya*

School of Chemistry, University of Hyderabad, Hyderabad-500046, India

Received February 12, 2001

Two new porphyrin arrays—a hexamer and a nonamer—have been synthesized and characterized by elemental analysis as well as mass, ^{1}H NMR, and UV−vis spectroscopic methods. The scheme of construction of these arrays employs a synthetic protocol involving sequential "organic" and "inorganic" reactions conducted, respectively, at the peripheral *meso*-phenyl ring and the central tin(IV) ion of the porphyrin scaffold. The architecture of the hexamer is such that it is based on a covalently linked tin(IV) porphyrin dimer, with each of the two tin(IV) centers *trans*-axially ligated to two free-base porphyrins, while the higher homologue features a tin(IV) porphyrin trimer as the basal unit, with its central metalloid ions having two free-base porphyrins as axial ligands. This extended, "axial-bonding"-type architecture of the new arrays has been investigated by the ^{1}H NMR method, which reveals characteristic ring-current-induced shifts and coupling patterns for the resonances due to protons of the axial free-base porphyrin subunits. The presence of any ring−ring (basal−basal, basal−axial, or axial−axial) interaction in these arrays is not obvious from their UV−vis and redox potential data, which are close to those of the corresponding constituent monomeric species. On the other hand, their singlet-state activities are quite different from those of the precursor reference compounds as probed by steady-state fluorescence. The results of the detailed investigations carried out on these hybrid, "bichromophoric" arrays have been interpreted in terms of the occurrence of intraarray, interchromophore energy- and electron-transfer reactions.

Introduction

Porphyrin arrays are useful in many research areas encompassing biomimetic photosynthesis, molecular electronics, molecular catalysis, etc.[1−3] Most of the porphyrin arrays reported so far have been synthesized via typical organic reaction sequences carried out at the porphyrin peripheral (i.e., pyrrole β or *meso*) position(s).[4−21] In recent years, "inorganic" reactions that can be conducted at the axial sites of porphyrin-bound metal ions[22] have also been employed for the construction of metalloporphyrin arrays.[23−32] Adapting this latter "axial-bonding" strategy and utilizing the well-known oxophilicity of metalloid ions, we have constructed a series of trimers based on phosphorus(V), tin(IV). or germanium(IV) porphyrin scaffolds.[33,34]

* To whom correspondence should be addressed. E-mail: bgmsc@uohyd.ernet.in.

(1) Wojaczynski, J.; Latos-Grazynski, L. *Coord. Chem. Rev.* **2000**, *204*, 113.
(2) Gust, D.; Moore, T. A. In *Handbook of porphyrins and related macrocycles*; Kadish, K. M., Guilard, R., Smith, K. M., Eds.; Academic Press: New York, 1999; Vol. 8, pp 153−190.
(3) Sanders, J. K. M. In *Handbook of porphyrins and related macrocycles*; Kadish, K. M., Guilard, R., Smith, K. M., Eds.; Academic Press: New York, 1999; Vol. 3, pp 347−368.
(4) Tsuda, A.; Furuta, H.; Osuka, A. *Angew. Chem., Int. Ed*. **2000**, *39*, 2549.
(5) Blake, I. M.; Rees, L. H.; Claridge, T. D. W.; Anderson, H. L. *Angew. Chem., Int. Ed*. **2000**, *39*, 1818.
(6) Masiero, S.; Gottarelli, G.; Pieraccini, S. *Chem. Commun. (Cambridge)* **2000**, 1995.
(7) Nagata, N.; Kugimiya, S.-I.; Kobuke, Y. *Chem. Commun. (Cambridge)* **2000**, 1389.
(8) Sugiura, K.-I,; Fujimoto, Y.; Sakata, Y. *Chem. Commun. (Cambridge)* **2000**, 1105.
(9) Hecht, S.; Emrick, T.; Frechet, J. M. *Chem. Commun. (Cambridge)* **2000**, 313.
(10) Kato, T.; Maruo, N.; Akisada, H.; Arai, T.; Nishino, N. *Chem. Lett.* **2000**, 890.
(11) Kondo, M.; Kimura, Y.; Wada, K.; Mizutani, T.; Ito, Y.; Kitagawa, S. *Chem. Lett.* **2000**, 818.
(12) Kato, T.; Uchiyana, M.; Maruo, N.; Arai, T.; Nishino, N. *Chem. Lett.* **2000**, 144.
(13) Mongin, O.; Hoyler, N.; Gossauer, A. *Eur. J. Org. Chem*. **2000**, 1193.
(14) Webb, S. J.; Sanders, J. K. M. *Inorg. Chem.* **2000**, *39*, 5920.
(15) Harmjanz, M.; Scott, M. J. *Inorg. Chem.* **2000**, *39*, 5428.
(16) Kuroda, Y.; Sugou, K.; Sasaki, K. *J. Am. Chem. Soc.* **2000**, *122*, 7833.
(17) Lammi, R. K.; Ambroise, A.; Balasubramanian, T.; Wagner, R. W.; Bocain, D. F.; Holten, D.; Lindsey, J. S. *J. Am. Chem. Soc.* **2000**, *122*, 7579.
(18) Kuebler, S. M.; Denning, R. G.; Anderson, H. L. *J. Am. Chem. Soc.* **2000**, *122*, 339.
(19) Blanco, M.-J.; Chambron, J.-C.; Heitz, V.; Sauvage, J.-P. *Org. Lett.* **2000**, *2*, 3051.
(20) Ravikanth, M. *Tetrahedron Lett.* **2000**, *41*, 3709.
(21) Li, J.; Ambroise, A.; Yang, S. K.; Diers, J. R.; Seth, J.; Wack, C. R.; Bocian, D. F.; Holten, D.; Lindsey, J. S. *J. Am. Chem. Soc.* **1999**, *121*, 8927 and references therein.
(22) Porphyrin arrays have also been built utilizing axial ligation of the porphyrin peripheral sites to non-porphyrinic metal centers. See, for example: Diskin-Posner, Y.; Dahal, S.; Goldberg, I. *Chem. Commun. (Cambridge)* **2000**, 585. Alessio, E.; Ciani, E.; Iengo, E.; Kukushkin, V. Y.; Marzilli, L. G. *Inorg. Chem*. **2000**, *39*, 1434.
(23) Redman, J. E.; Feeder, N.; Teat, S. J.; Sanders, J. K. M. *Inorg. Chem*. **2001**, *40*, 2486.
(24) Ogawa, K.; Kobuke, Y. *Angew. Chem., Int. Ed.* **2000**, *39*, 4070.
(25) Haycock, R. A.; Yartsev, A.; Michelsen, U.; Sundstrom, V.; Hunter, C. A. *Angew. Chem., Int. Ed.* **2000**, *39*, 3616.
(26) Sakamoto, M.; Ueno, A.; Mihara, H. *Chem. Commun. (Cambridge)* **2000**, 1741.
(27) Chichak, K.; Branda, N. R. *Chem. Commun. (Cambridge)* **2000**, 1211.
(28) Felluga, F.; Tecilla, P.; Hillier, L.; Hunter, C. A.; Licini, G.; Scrmin, P. *Chem. Commun. (Cambridge)* **2000**, 1087.
(29) Hamstra, B. J.; Cheng, B.; Ellison, M. K.; Scheidt, W. R. *Inorg. Chem.* **2000**, *39*, 1454.
(30) Ikeda, C.; Nagahara, N.; Yoshioka, N.; Inoue, H. *New J. Chem*. **2000**, *24*, 897.
(31) Ambroise, A.; Li, J.; Yu, L.; Lindsey, J. S. *Org. Lett.* **2000**, *2*, 2563.
(32) Kim, H.-J.; Bampos, N.; Sanders, J. K. M. *J. Am. Chem. Soc.* **1999**, *121*, 1, 8120 and references therein.
(33) Rao, T. A.; Maiya, B. G. *J. Chem. Soc., Chem. Commun*. **1995**, 939.

10.1021/ic010179u CCC: $20.00
Published on Web 11/14/2001

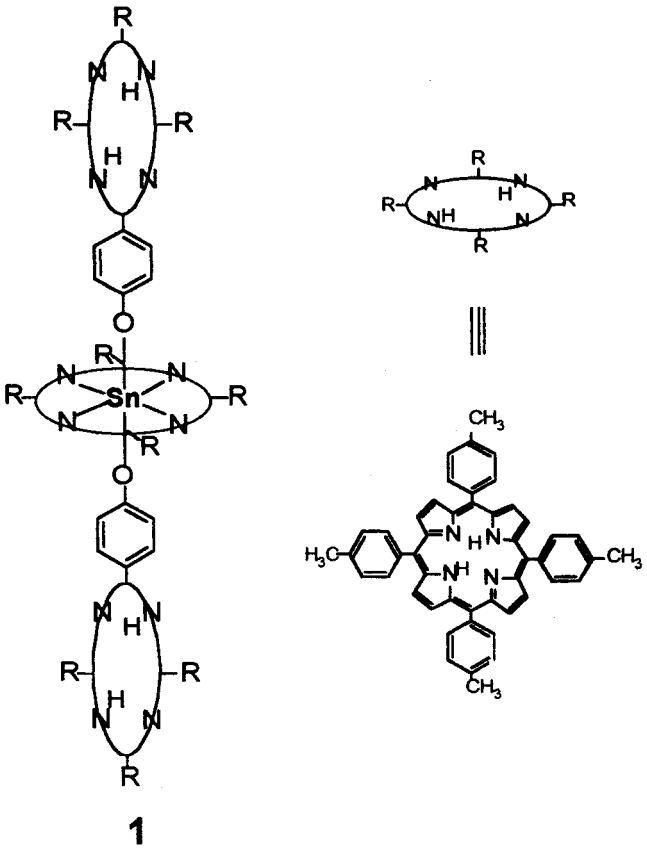

Figure 1. Structure of the axial-bonding-type trimer **1**.

The structure of a representative, axial-bonding-type trimer, viz., **1**, is shown in Figure 1.[35] During the course of these investigations, we realized that it should be possible to synthesize more elaborate arrays having diverse structures and functions by utilizing the reactivities at both the peripheral and axial sites of a metalloid porphyrin species. Recently, we were able to accomplish this goal and to synthesize two higher (than **1**) oligomers, viz., hexamer **6** and nonamer **9** illustrated in Figures 2 and 3, respectively. As seen in these figures, while a typical organic reaction (ether formation) involving the porphyrin peripheral hydroxy group(s) was employed for the propagation of these arrays in the lateral direction, the oxophilic nature of the tin center was advantageously utilized for their expansion in the axial direction.[36] The details of the design, construction, spectral characterization, and redox as well as singlet-state properties of **6** and **9** are reported in this paper.

(34) Giribabu, L.; Rao, T. A.; Maiya, B. G. *Inorg. Chem*. **1999**, *38*, 4971.

(35) The nomenclature of the various porphyrin arrays discussed here is as follows: **1**, (free-base porphyrin)$_2$(tin(IV) porphyrin) ≡ [(TTP)-$Sn^{IV}(H_2TriTP(O))_2$]; **4**, (H_2TriTP)−$O(CH_2)_2O$−(H_2TriTP); **5**, [(TriTP)-$Sn^{IV}(OH)_2$]−$O(CH_2)_2O$−[(TriTP)$Sn^{IV}(OH)_2$]; **6**, [(TriTP)$Sn^{IV}(H_2$-$TriTP(O))_2$]−$O(CH_2)_2O$−[(TriTP)$Sn^{IV}(H_2TriTP(O))_2$]; **7**, (H_2TriTP)−$O(CH_2)_3O$−(H_2DiTP)−$O(CH_2)_3O$−(H_2TriTP); **8**, [(TriTP)$Sn^{IV}(OH)_2$]−$O(CH_2)_3O$−[(DiTP)$Sn^{IV}(OH)_2$]−$O(CH_2)_3O$−[(TriTP)$Sn^{IV}(OH)_2$]; **9**, [(TriTP)$Sn^{IV}(H_2TriTP(O))_2$]−$O(CH_2)_3O$−[(DiTP)$Sn^{IV}(H_2TriTP(O))_2$]−$O(CH_2)_3O$−[(TriTP)$Sn^{IV}(H_2TriTP(O))_2$]. Here, H_2TriTP(O) refers to the axial free-base porphyrin that is linked to the basal tin(IV) center via its *meso*-phenoxy group, and (DiTP) appearing in the formulas for **7**, **8**, and **9** corresponds to the central ditolylporphyrin in each case. The linkers $-O(CH_2)_2O-$ and $-O(CH_2)_3O-$, separating the basal porphyrins, need to be assumed to originate from the *meso*-phenyl rings. See Figure 2 for the structures of **4**, **5**, and **6** and Figure 3 for the structures of **7**, **8**, and **9**.

(36) The oxophilicity of the tin(IV) centers has recently been employed for the construction of heterobimetallic porphyrin trimers (ref 23 and Maiya, B. G.; Bampos, N.; Kumar, A. A.; Feeder, N.; Sanders, J. K. M. *New. J. Chem* **2001**, 797).

Experimental Section

The chemicals and solvents utilized in this study were purchased from either Aldrich Chemical Co. or BDH (Mumbai, India). The solvents utilized for spectroscopic and electrochemical experiments were further purified using standard procedures.[37]

A. Synthesis. Monomers 5,10,15,20-tetra(*p*-tolyl)porphyrin (H_2-TTP),[38] [5,10,15,20-tetra(*p*-tolyl)porphyrinato]tin(IV) dihydroxide ([(TTP)-$Sn^{IV}(OH)_2$]),[39] 5,10,15,20-tetraphenylporphyrin (H_2TPP),[38] (5,10,15,20-tetraphenylporphyrinato)zinc(II) ([(TPP)Zn^{II}]),[40] 5,10,15-tri(*p*-tolyl)-20-(4-hydroxyphenyl)porphyrin (**2a**),[41] 5,15-bis(4-hydroxyphenyl)-10,20-bis(*p*-tolyl)porphyrin (**3a**),[42] 5,10,15-tri(*p*-tolyl)-20-[4-(2-bromoethoxy)phenyl]porphyrin (**2b**),[43] and 5,10,15-tri(*p*-tolyl)-20-[4-(3-bromo-1-propoxy)phenyl]porphyrin (**3b**)[43] were synthesized according to the reported procedures.

5,10,15-Tri(*p*-tolyl)-20-[4-[2-[4-[10,15,20-tri(*p*-tolyl)-5-porphyrinyl]phenoxy]ethoxy]phenyl]porphine (4).

This free-base porphyrin dimer was prepared by stirring compounds **2a** and **2b** in the DMF/K_2CO_3 milieu for 48 h and was purified by chromatographic separation (alumina, $CHCl_3$) followed by recrystallization (CH_2Cl_2–hexane), as reported.[43]

[*μ*-[5,10,15-Tri(*p*-tolyl)-20-[4-[2-[4-[10,15,20-tri(*p*-tolyl)-5-porphyrinyl]phenoxy]ethoxy]phenyl]porphyrinato]]ditin(IV) Tetrahydroxide (5).

A mixture containing free-base dimer **4** (0.20 g 0.15 mmol) and $SnCl_2$ (0.50 g, 2.23 mmol) in pyridine (20 mL) was refluxed for 2 h, after which 10 mL of aqueous ammonia (25%, v/v) was added. The resulting solution was stirred for 1 h at 50 °C. Solvent pyridine was removed under reduced pressure, and the solid obtained was taken up in $CHCl_3$. The organic layer, after being washed several times with water, was dried by being passed through anhydrous Na_2SO_4 and chromatographed over basic alumina. Elution with $CHCl_3$−CH_3OH (98:2 v/v) furnished **5**, which was recrystallized from CH_2Cl_2−hexane. Yield: 0.22 g (92%). UV−vis (CH_2Cl_2): λ_{max}, nm (log ϵ) 428 (5.68), 562 (4.40), 606 (4.29). ^{1}H NMR ($CDCl_3$, TMS, 200 MHz): δ 9.19 (m, 16H), 8.34 (d, 4H, $J = 8.0$), 8.25 (d, 12H, $J = 7.6$), 7.65 (d, 12H, $J = 7.6$), 7.55 (d, 4H, $J = 8.0$), 4.65 (s, 4H), 2.78 (m, 18H). $E_{1/2}$ (CH_2Cl_2, 0.1 M TBAP), V vs SCE: −0.88,−1.02, 1.39.

Porphyrin Hexamer 6. A C_6H_6 (50 mL) solution containing 0.05 g (0.03 mmol) of **5** and 0.10 g (0.15 mmol) of **2a** was refluxed for 12 h under a nitrogen atmosphere. The solvent was evaporated in vacuo, and the resulting residue was dissolved in a minimum amount of $CHCl_3$ and loaded onto a neutral alumina column. Hexamer **6** was eluted with $CHCl_3$, after which it was recrystallized using a mixture of CH_2Cl_2–hexane. Yield: 82 mg (64%). Anal. Calcd for $C_{284}H_{210}O_6N_{24}Sn_2$: C, 79.45; H, 4.93; N, 7.83. Found: C, 78.33; H, 5.06, N, 7.34. MALDI-TOF MS: calcd 4292, found 4290. ^{1}H NMR ($CDCl_3$, TMS, 500 MHz): δ 9.39 (m, 16H), 8.82 (d, 16H, $J < 4.0$), 8.60 (d, 8H, $J = 4.2$), 8.34 (d, 16H, $J = 6.9$), 8.17 (d, 8H, $J = 4.2$), 8.01 (m, 24H), 7.51 (m, 40H), 6.56 (d, 8H, $J = 7.6$), 4.45 (s, 4H), 2.65 (m, 54H), 2.44 (d, 8H, $J = 7.6$), −2.91 (s, 8H).

Free-Base Trimer 7. A mixture containing the *trans*-dihydroxyporphyrin **3a** (0.20 g, 0.30 mmol), bromide **3b** (2.38 g, 3 mmol), and 0.5 g of anhydrous K_2CO_3 in 50 mL of DMF was stirred magnetically for 72 h at room temperature under a nitrogen atmosphere. The product was precipitated by pouring the reaction mixture onto 100 mL of 10% aqueous methanolic solution. The precipitate was filtered off and dried under vacuum. The solid obtained was chromatographed (neutral alumina). Elution with $CHCl_3$−hexane (50:50 v/v) gave unreacted **3b**, after which free-base trimer **7** was eluted with $CHCl_3$. It was

(37) Perrin, D. D.; Armarego, W. L. F.; Perrin, D. R. *Purification of laboratory Chemicals*; Pergamon: Oxford, 1986.

(38) Lindsey, J. S.; Schreiman, I. C.; Hsu, H. C.; Kearney, P. C.; Marguerettaz, A. M. *J. Org. Chem.* **1987**, *52*, 827.

(39) Kadish, K. M.; Xu, Q. Y. Y.; Maiya, B. G.; Barbe, J.-M.; Guilard, R. *J. Chem. Soc., Dalton Trans*. **1989**, 1531.

(40) Fuhrhop, J.-H.; Smith, K. M. In *Porphyrins and Metalloporphyrins*; Smith, K. M., Ed.; Elsevier: Amsterdam, 1975; p 769.

(41) Moghadam, G. E.; Ding, L.; Tadj, F.; Meunier, B. *Tetrahedron* **1989**, *45*, 2641.

(42) Lee, C.-H.; Lindsey, J. S. *Tetrahedron* **1994**, *50*, 11427.

(43) Little, R. G. *J. Heterocycl. Chem*. **1978**, *15*, 203.

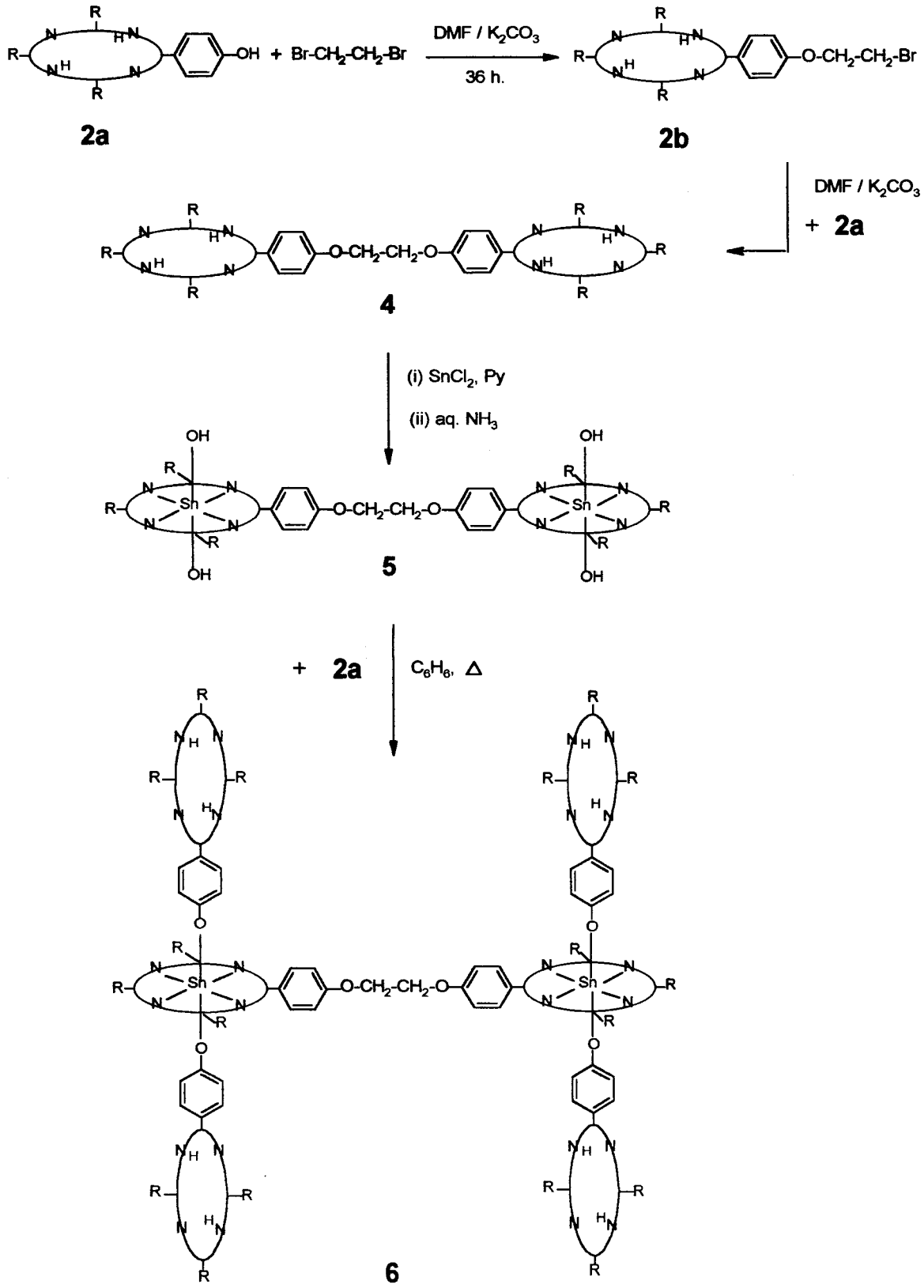

Figure 2. Scheme leading to the synthesis of hexamer **6**.

recrystallized from CH_2Cl_2−hexane. Yield: 0.29 g (46%). UV−vis (CH_2Cl_2): λ_{max}, nm (log ϵ) 420 (5.46), 517 (4.11), 553 (4.02), 592 (3.88), 648 (3.80). ^{1}H NMR ($CDCl_3$, TMS, 200 MHz): δ 8.89 (m, 24H), 8.12 (m, 24H), 7.48 (m, 24H), 4.63 (t, 8H), 2.78 (m, 28H), −2.72 (s, 6H). $E_{1/2}$ (CH_2Cl_2, 0.1 M TBAP), V vs SCE: −1.14, −1.45, 1.02, 1.39.

Tin(IV) Trimer 8. A mixture containing **7** (0.21 g, 0.10 mmol) and $SnCl_2$ (0.50 g, 2.23 mmol) in pyridine (20 mL) was refluxed for 2 h, after which 10 mL of aqueous ammonia (25%, v/v) was added. The resulting solution was stirred for 1 h at 50 °C. Solvent pyridine was removed under reduced pressure, and the solid obtained was purified as described above for **5** to obtain **8**. Yield: 0.22 g (88%). UV−vis

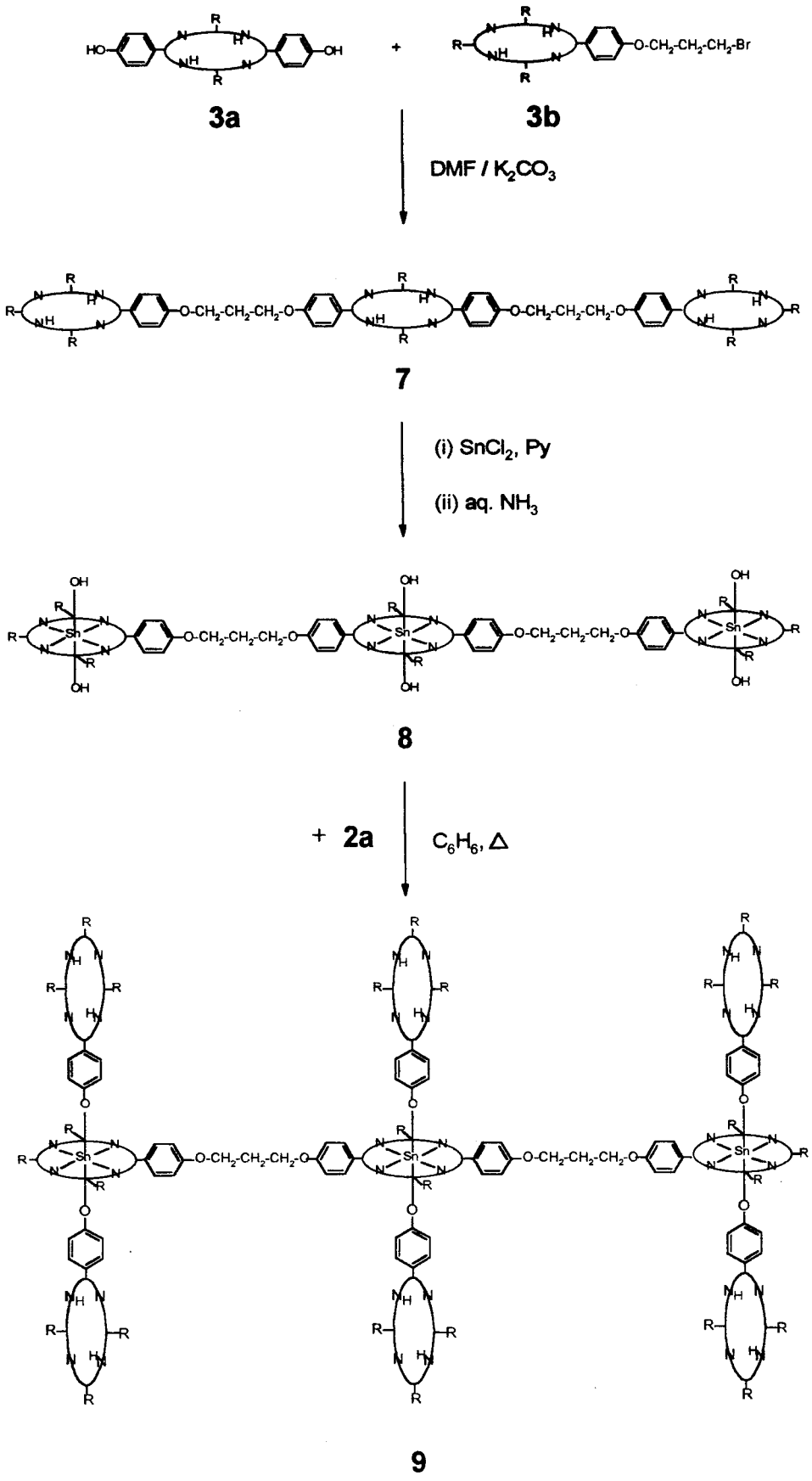

Figure 3. Scheme leading to the synthesis of nonamer **9**.

(CH_2Cl_2): λ_{max}, nm (log ϵ) 430 (5.70), 564 (4.40), 605 (4.39). ^{1}H NMR ($CDCl_3$, TMS, 200 MHz): δ 9.15 (m, 24H), 8.23 (m, 24H), 7.55 (m, 24H), 4.65 (t, 8H), 2.69 (m, 28H). $E_{1/2}$ (CH_2Cl_2, 0.1 M TBAP), V vs SCE: −0.89, −1.27, 1.44.

Nonamer 9. Trimer **8** (0.05 g, 0.02 mmol) and monomer **2a** (0.20 g, 0.30 mmol) were dissolved in dry C_6H_6 (20 mL), and the contents were refluxed for 12 h under a nitrogen atmosphere. Evaporation of the solvent and purification of the residue by preparative TLC on neutral alumina (solvent $CHCl_3$) afforded **9**. It was recrystallized from CH_2Cl_2–hexane. Yield: 43 mg (34%). Anal. Calcd for $C_{428}H_{318}O_{10}N_{36}Sn_3$: C, 79.31; H, 4.94; N, 7.78. Found: C, 78.31; H, 5.06; N, 7.61. MALDI-TOF MS: calcd 6477, found 6482. ^{1}H NMR ($CDCl_3$, TMS, 500 MHz): δ 9.35 (m, 24H), 8.75 (m, 24H), 8.51 (d, 12H, $J = 5.0$), 8.30 (d, 24H, $J = 7.0$), 8.15 (d, 12H, $J = 5.0$), 7.98 (m, 36H), 7.43 (m, 60H), 6.55 (d, 12H, $J = 7.9$), 4.28 (m, 8H), 2.62 (m, 82H), 2.40 (d, 12H, $J = 7.9$), −2.90 (s, 12H).

B. Methods. MALDI-TOF spectra were recorded on a Kompact MALDI 4 mass spectrometer (Kratos Analytical Ltd.). The instrument was operated in reflection time-of-flight mode with an accelerating potential of 20 kV and in the negative ion recording mode. Elemental analysis was carried out with the Perkin-Elmer model 240-C CHN analyzer.

UV−vis spectra were recorded with a Shimadzu model UV-3101-PC UV−vis spectrophotometer. The concentration of the samples used for these measurements ranged from $\sim 2 \times 10^{-6}$ M (Soret bands) to $\sim 5 \times 10^{-5}$ M (Q-bands). Steady-state fluorescence spectra were recorded using a Jasco model FP-777 spectrofluorimeter. The emitted quanta were detected at right angles to the incident beam. The utilized concentrations of the fluorophores were such that the optical densities (ODs) at the excitation wavelengths were always less than 0.2. The fluorescence quantum yields (ϕ) were estimated by integrating the areas under the fluorescence curves and by using H_2TPP ($\phi = 0.11$ in CH_2Cl_2) or [(TPP)Zn^{II}] ($\phi = 0.036$ in CH_2Cl_2) as the standard.[44,45] Refractive index corrections have been incorporated while reporting the fluorescence data in various solvents. Dilute solutions ($\sim 10^{-7}$ M) of the fluorophores were utilized for the excitation spectral measurements. Corrections to the instrument response (up to 650 nm) and procedures for the spectral normalization employed during the estimations of the excitation energy transfer efficiencies are essentially similar to those described in our previous studies.[34,46,47] ^{1}H NMR (1D and 2D COSY) spectra were recorded with a Bruker NR-200 or DRX-500 spectrometer using $CDCl_3$ as the solvent and tetramethylsilane (TMS) as the internal standard. The chemical shift (δ) and coupling constant (J) values are given in parts per million and hertz, respectively, throughout this paper.

Cyclic voltammetric experiments (CH_2Cl_2 and 0.1 M tetrabutylammonium perchlorate, TBAP) were performed on a Princeton Applied Research (PAR) 174A polarographic analyzer coupled with a PAR 175 universal programmer and a PAR RE 0074 $x-y$ recorder, as detailed in our previous studies.[34,46−51] The Fc^+/Fc couple (Fc = ferrocene) was used to calibrate the redox potential values.

Care was taken to avoid the entry of direct, ambient light into the samples in all the spectroscopic and electrochemical experiments. Unless otherwise specified, all the experiments were carried out at 293 ± 3 K.

Results and Discussion

A. Design and Synthesis. The majority of established methods that are available for the construction of porphyrin arrays involve *either* manipulation at the porphyrin peripheral position(s) *or* axial ligation at the central metal/metalloid ion. In the present study, relying on a "building block" approach, synthesis of arrays **6** and **9** has been achieved by employing sequential "organic" and "inorganic" reactions.[52] Indeed, from a retrosynthetic viewpoint, whereas propagation of these "branched-chain"-type arrays in the lateral direction involves typical ether bond formation reaction, construction of the perpendicular "branches" employs the "axial-bonding" capability of the central, oxophilic tin(IV) ion.

The precursor porphyrin building blocks necessary for the construction of hexamer **6** (i.e., **2a**, **2b**, and **4**) and nonamer **9** (i.e., **3a** and **3b**) were prepared by closely following the corresponding methods reported in the literature.[38−43] The ditin dimer **5** was synthesized in high yield by reacting **4** with $SnCl_2$ in refluxing pyridine for 2 h followed by treatment with aqueous ammonia. This dimer, with the two axial hydroxy ligands amenable for further reaction on each of its tin(IV) centers, reacted smoothly with excess **2a** in refluxing dry C_6H_6 to afford the axial-bonding-type hexameric array **6** in 64% yield, Figure 2. The synthesis of nonamer **9** also followed a similar strategy in that it was constructed in a stepwise manner starting from the *trans*-dihydroxyporphyrin **3a** as the basic building block. Reaction of **3a** with bromide **3b** in the K_2CO_3/DMF milieu and purification afforded trimer **7**, which upon tin insertion by the standard method furnished **8** in a moderate overall yield. Nonamer **9** was obtained by the reaction of **8** and excess **2a** following a procedure analogous to that described above for the synthesis of **6**, Figure 3. It should be noted here that we have connected the basal porphyrin units in **9** by three methylene groups as compared to two in **6**. This was done to avoid any possible steric clash between the axial porphyrin ligands on the "central" tin(IV) porphyrin and the corresponding ligands on the two "peripheral" tin(IV) porphyrins in this "crowded" array.

B. Spectral and Electrochemical Characterization. The UV−vis, ^{1}H NMR, and electrochemical data of the precursor porphyrins **5**, **7**, and **8** are summarized in the Experimental Section (see the Supporting Information for the spectra). The new arrays **6** and **9** were found to be quite soluble in most organic solvents and easily amenable for characterization by elemental analysis and mass, UV−vis, and ^{1}H NMR spectroscopic methods. The elemental analysis and mass and ^{1}H NMR spectral data of both the arrays are provided in the Experimental Section.

The ^{1}H NMR spectrum of array **6** is illustrated in Figure 4 along with the proton assignments, which are made on the basis of the ^{1}H NMR data of the trimeric array **1**[34] and on examination of the ^{1}H−^{1}H COSY spectral features. Of specific interest in this regard are the *meta* (type e) and *ortho* (type f) protons of the phenoxo groups of the free-base porphyrins that are bound to the tin center. These protons, being affected by both the inherent deshielding effect of the axial porphyrin and the shielding effect of the basal porphyrin,[53] resonate at 6.56 (d, 8H) and 2.44 (d, 8H, $^3J_{HH} = 7.6$ Hz) ppm, respectively, as detected by the proton connectivity pattern in the ^{1}H−^{1}H COSY spectrum (see the inset in Figure 4). The inner imino protons of the axial free-base porphyrins (type k) of **6** are seen to experience the "long-range" shielding effect due to the ring current of the basal tin(IV) porphyrin and resonate at −2.91 ppm (s, 8H) compared to the corresponding −NH protons of **2a** that appear at −2.73 ppm.

The general resonance pattern observed in the ^{1}H NMR spectrum of **9** is quite similar to that observed for **6**. The

(44) Quimby, D. J.; Longo, F. R. *J. Am. Chem. Soc.* **1975**, *19*, 5111.
(45) Harriman, A.; Davila, J. *Tetrahedron* **1989**, *45*, 4737.
(46) Sirish, M.; Kache, R.; Maiya, B. G. *J. Photochem. Photobiol., A* **1996**, *93*, 129.
(47) Sirish, M.; Maiya, B. G. *J. Photochem. Photobiol., A* **1995**, *88*, 127.
(48) Rao, T. A.; Maiya, B. G. *Inorg. Chem.* **1996**, *35*, 4829.
(49) Ambroise, A.; Maiya, B. G. *Inorg. Chem.* **2000**, *39*, 4256.
(50) Ambroise, A.; Maiya, B. G. *Inorg. Chem.* **2000**, *39*, 4264.
(51) Hariprasad, G.; Dahal, S.; Maiya, B. G. *J. Chem. Soc., Dalton Trans.* **1996**, 3429.
(52) Recently, a combined covalent and coordination approach to dendritic multiporphyrin arrays based on ruthenium(II)/rhodium(III) porphyrins has been developed by Sanders and co-workers (ref 23 and Darling, S.; Mak, C. C.; Bampos, N.; Feeder, N.; Teat, S. J.; Sanders, J. K. M. *New J. Chem.* **1999**, *23*, 359).
(53) Abraham, R. J.; Bedford, G. R.; McNeillie, D.; Wright, B. *Org. Magn. Reson*. **1980**, *14*, 418.

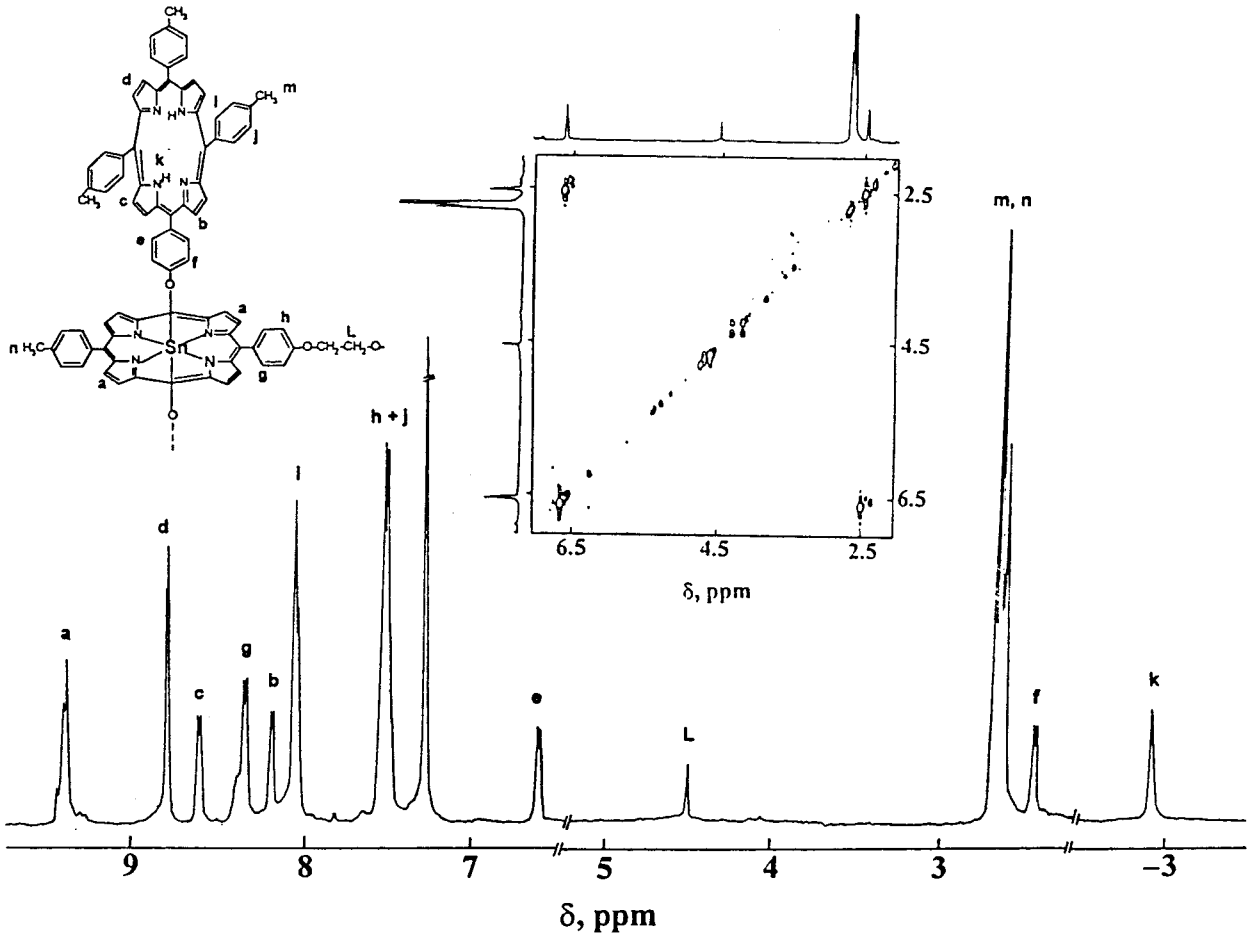

Figure 4. ^{1}H NMR spectrum ($CDCl_3$, TMS) of the hexamer **6** along with the various proton assignments. The inset shows the partial ^{1}H−^{1}H COSY spectrum, clearly illustrating the cross-peaks resulting from coupling of the spacer *meta* (e) and *ortho* (f) protons.

shielding/deshielding effects experienced by the various protons on all six axial free-base porphyrins of this nonamer are also similar to those described above for the corresponding protons on the hexamer. In principle, the four "external" axial free-base porphyrins of this array should be different from the two which are bound to the central tin(IV) porphyrin, but this effect was not obvious in the NMR spectrum under the present experimental conditions. However, the multiplet that is ascribable to the pyrrole β proton resonances of the basal tin(IV) porphyrins of this array (9.35 ppm, 24H) is more complex than the corresponding resonances of hexamer **6**, suggesting that the central tin(IV) macrocycle is different from the two external tin(IV) porphyrins.

An additional concern with this class of octahedral tin(IV) complexes is the lability of the axial bonds and was indeed investigated earlier by the NMR method for tin(IV) porphyrins having inorganic or organic ligands.[54−56] Specifically, ^{1}H NMR studies carried out earlier on $[(P)Sn^{IV}(OC(O)A)_2]$ (where P is a tetraarylporphyrin and OC(O)A is the axially ligated anthracene-9-carboxylate subunit) have revealed, in addition to the $\pi-\pi$ interaction between the porphyrin and anthracene rings, the presence of ligand on−off equilibrium.[56] In contrast, neither the $\pi-\pi$ interaction nor the ligand on−off equilibrium was discernible from the NMR data of both **6** and **9**. This observation indicates that, under our experimental conditions, the two *trans* free bases are strongly bound in a symmetric manner at each tin(IV) center in these systems as is the case with the previously investigated array **1**. In addition, the fact that the resonance positions of the various protons of the axial free-base ligands present in **6** and **9** are close to those of the corresponding protons of **1** suggests that the interaction between the axial rings bound to two different tin(IV) centers is minimal in the higher arrays. We, however, note that free rotations about the axial Sn−O bonds cannot be altogether neglected in these axial-bonding-type arrays. The issues concerning the axial bond rotation and the conformational equilibria that are possible in these arrays can be addressed with the help of variable-temperature NMR data, but such experiments have not been carried out during the present study.

The UV−vis spectra of the two new arrays are compared in Figure 5. The UV−vis data of these arrays as well as those of the corresponding reference compounds trimer **1** and monomers **2a** and $[(TTP)Sn^{IV}(OH)_2]$ are summarized in Table 1. Inspection of these data and those obtained for the spectrum of a solution containing 1:2 (mol/mol) equiv of **2a** and $[(TTP)Sn^{IV}(OH)_2]$ reveals that, within experimental error, the peak maxima (λ_{max}) of both **6** and **9** are close to each other, in addition to being close to the λ_{max} values of the physical mixture containing the reference compounds mentioned above. Moreover, the molar absorptivities at the peak maxima (ϵ) of the arrays are also nearly equal to the sum of those due to their constituent partners (Table

(54) Kadish, K. M.; Xu, Q. Y. Y.; Maiya, B. G.; Barbe, J.-M.; Guilard, R. *J. Chem. Soc., Dalton Trans.* **1989**, 1531.
(55) Hawley, J. C. Ph.D. Thesis, University of Cambridge, Cambridge, U.K., 1998.
(56) Hawley, J. C.; Bampos, N.; Abraham, R. J.; Sanders, J. K. M. *Chem. Commun.* **1998**, 661.

Table 1. UV−Vis and Redox Potential Data

compd	UV−vis data,[a] λ_{max}, nm (log ϵ)					redox data,[b] potential, V vs SCE	
	main B-band	Q-bands				reduction	oxidation
9	422 (5.99)	519 (4.69)	560 (4.70)	604 (4.52)	650 (4.29)	−0.96, −1.28, −1.47,[c] −1.68	0.83, 1.37[c]
6	420 (5.83)	519 (4.56)	561 (4.59)	604 (4.49)	651 (4.26)	−0.93, −1.25, −1.46,[c] −1.66	0.90, 1.43[c]
1[d]	420 (5.77)	518 (4.64)	559 (4.64)	603 (4.62)	650 (3.60)	−1.00, −1.32, −1.49,[c] −1.64	0.93, 1.24[c]
2a	418 (5.30)	516 (4.17)	551 (3.90)	592 (3.64)	650 (3.56)	−1.24, −1.64[c]	0.94, 1.30
[(TTP)$Sn^{IV}(OH)_2$]	428 (5.56)	524 (3.56)	563 (4.43)	603 (4.52)		−0.88, −1.02	1.39[c]

[a] Solvent CH_2Cl_2. Error limits: λ_{max}, ±1 nm; ϵ, ±6%. [b] Measured in CH_2Cl_2, 0.1 M TBAP. Error limits ±0.03 V. [c] Quasi-reversible/irreversible. [d] Taken from ref 34.

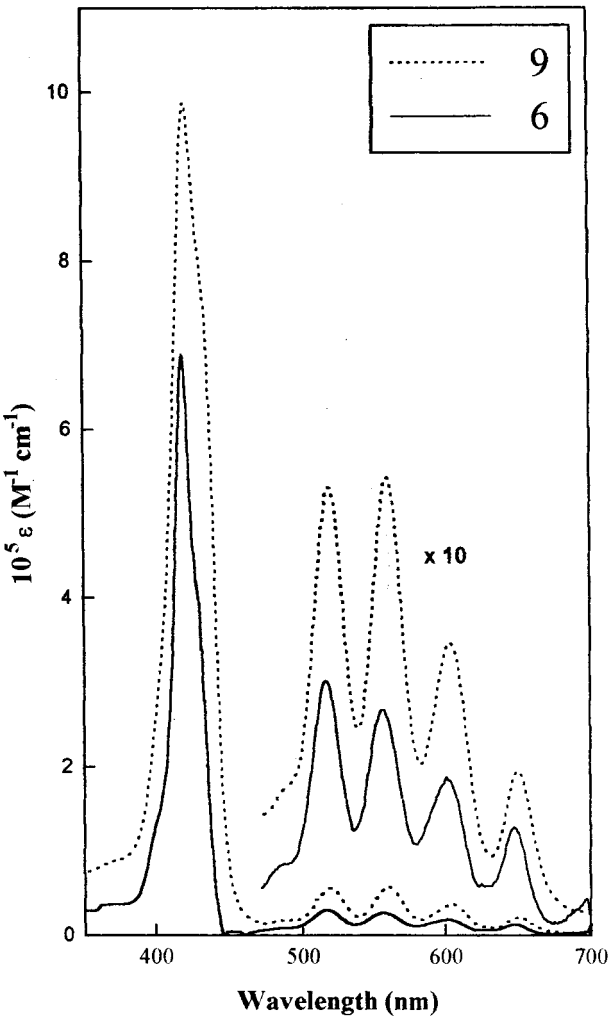

Figure 5. UV−vis spectra of the two arrays investigated in this study.

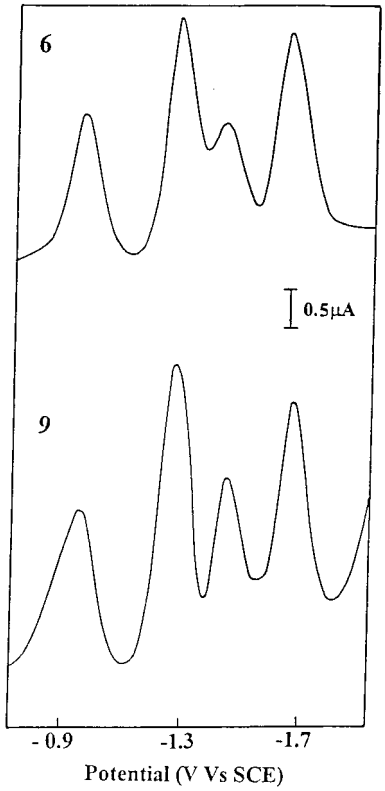

Figure 6. Differential pulse voltammograms of the arrays in CH_2Cl_2, 0.1 M TBAP (scan rate 10 mV s^{-1}, modulation amplitude 10 mV).

1).[57] These observations clearly indicate that there is minimal perturbation of the electronic structures of the individual macrocyclic π-systems in these arrays. Specifically, there exists no indication of the presence of exciton coupling between the porphyrin rings (i.e., axial−axial, axial−basal, or basal−basal).

The electrochemical redox potentials, as measured from the cyclic and differential pulse voltammetric measurements, also reveal the absence of electronic interaction between the various porphyrin rings in both **6** and **9**. Figure 6 shows the differential pulse voltammograms obtained during the anodic scan, and Table 1 provides the redox potential data of **9**, **6**, **1,** and the corresponding monomeric species. Each array undergoes up to four reduction steps and up to two oxidation steps in CH_2Cl_2, 0.1 M TBAP. Wave analysis (cyclic voltammetry) suggested that while the first oxidation and also the first two reduction steps are reversible,[59] diffusion-controlled and one-electron-transfer reactions, the subsequent steps are, in general, either quasi-reversible or totally irreversible.[58] On the basis of the redox potential data of the individual monomers (i.e., **2a** and [(TTP)$Sn^{IV}(OH)_2$]) and also that of [(TTP)$Sn^{IV}(OPh)_2$] (where OPh is the axially ligated phenoxy group), we have attempted to assign the midpoint potentials to basal and axial porphyrins separately. Analysis of the data reveals that the redox potentials of the hybrid arrays are in the same range as those of their corresponding monomeric analogues or the precursor dimeric/trimeric porphyrins (see the Experimental Section) as is the case with **1** (see Table 1) reported earlier.[34]

(57) However, note that ϵ for the various peaks follow the order trimer < hexamer < nonamer, as expected.

(58) Reversible peaks are characterized by the following: $i_{pc}/i_{pa} = 0.9-1.0$, $i_{pc}/\nu^{1/2}$ = constant in the scan rate (ν) range 50−500 mV/s, and $\Delta E_P = 60-70$ mV ($\Delta E_P = 65 \pm 3$ mV for the ferrocene$^+$/ferrocene couple). Quasi-reversible peaks are characterized by the following: $E_{pa} - E_{pc} = 90-200$ mV and $i_{pc}/i_{pa} = 0.5-0.8$ in the scan rate (ν) range 100−500 mV/s (see ref 59). Here, i_{pc}, E_{pc}, i_{pa}, and E_{pa} are the cathodic peak current and potential and the anodic peak current and potential, respectively. ΔE_P is the potential separation between the anodic and cathodic peaks.

(59) Nicholson, R. S.; Shain, I. *Anal. Chem.* **1964**, *36*, 706.

Table 2. Fluorescence Data[a]

	λ_{em}, nm (%Q)[b]					
	toluene		CH_2Cl_2		DMF	
array	λ_{ex} = 405 nm	λ_{ex} = 445 nm	λ_{ex} = 405 nm	λ_{ex} = 445 nm	λ_{ex} = 405 nm	λ_{ex} = 445 nm
9	657, 720 (97)	657, 719 (100)	656, 720 (94)	657, 717 (100)	658, 719 (94)	657, 718 (100)
6	657, 720 (93)	657, 720 (100)	656, 717 (91)	657, 718 (100)	657, 720 (88)	657, 719 (100)
1	658, 721 (82)	613, 658, 720 (95)	657, 719 (82)	613, 657, 719 (79)	656, 718 (92)	657, 720 (96)

[a] Error limits: λ_{em}, ±1 nm; %Q, ±10%. [b] %Q values for excitations at 445 (Q_1) and 405 (Q_2) nm are defined in refs 61 and 66, respectively.

Collectively, ^{1}H NMR, UV−vis, and redox potential data indicate that there exists a symmetric disposition of the two axial free-base porphyrins with respect to the plane of the corresponding basal tin(IV) porphyrin in these arrays. These data also indicate that there is no specific interaction between the neighboring axial free-base porphyrins in this class of soluble arrays. Notwithstanding this analysis, we emphasize that the structural drawings of **9**, **6**, and **1** as shown in Figures 1−3 do not convey the actual arrangement of the porphyrin rings. Specifically, we note that the Sn−O−C angles are not equal to 180°, as shown. Instead, it is likely that the free-base porphyrins might be somewhat diagonally disposed toward the tin(IV) porphyrins in these arrays as is the case with [(P)Sn^{IV}(ONap)$_2$] (where Nap is the axially ligated naphthyl subunit), the X-ray structure of which has been reported recently.[60] To date, our attempts to grow single crystals of these large arrays for the possible determination of their structures by X-ray crystallography have been unsuccessful.

C. Singlet-State Properties. When excited at 445 nm, the ditin dimer **5** and the tritin trimer **8** both showed a typical two-banded fluorescence spectrum in CH_2Cl_2, with the emission maxima appearing in the 615 (band I) and 667 (band II) nm region. The quantum yields of fluorescence (ϕ) of these tin(IV) porphyrin precursors were found to be close to that of the reference porphyrin [(TTP)Sn^{IV}(OH)$_2$] (ϕ = 0.048) as measured in the band I region. Excitation (λ_{exc} = 405 nm) of the precursor free-base porphyrins **2a**, **4**, and **7** also resulted in a two-banded spectrum, the emission maximum of the major band located in the band II region (655 nm) mentioned above and the minor band centered at ∼720 nm (band III) in each case. The fluorescence quantum yields of **4** and **7** were found to be nearly equal to that of **2a** (ϕ = 0.12). All of these data indicate that it is possible to individually address the singlet-state properties of the axial and basal porphyrins of arrays **6** and **9** as is the case with the trimer **1**.[34] Irradiation of these arrays at 405 nm should result in a predominant absorption by the axial free-base porphyrins, and that at 445 nm excites the central tin(IV) porphyrins. Moreover, fluorescence due to the tin(IV) and free-base components of the arrays can be exclusively monitored at bands I and III, respectively, with band II being common to both. Armed with this information, we carried out fluorescence studies with **6** and **9**, and the results reveal that, unlike the case with the ground-state properties, the singlet-state activities of these arrays are quite different from those of their precursor reference compounds, as described below.

1. Excitation at 445 nm. Excitation of toluene, CH_2Cl_2, or DMF solutions of **6** and **9** at 445 nm was seen to result in strong quenching of their fluorescence with respect to the fluorescence of [(TTP)Sn^{IV}(OH)$_2$]. In fact, the percent quenching (%Q_1)[61] is close to 100 in each investigated solvent, with band I that is characteristic of the tin(IV) porphyrin emission being totally absent in the spectra of these arrays (see Table 2). This total quenching of emission in these higher arrays is in contrast with the partial quenching observed when trimer **1** was excited under a similar set of experimental conditions of excitation wavelength and solvent, Figure 7. Inspection of this figure and the spectral data summarized in Table 2 reveals that while the spectrum of trimer **1** shows the presence of band I along with bands II and III, the spectra of both **6** and **9** are characterized by only bands II and III. It should be noted here that the appearance of bands II and III that are ascribable to the free-base porphyrin emission in the spectra of these three arrays when λ_{ex} = 445 nm is not due to the direct excitation of their axial free-base components.[62] Rather, it is a consequence of the excitation energy transfer (EET) from the central metalloid porphyrin to the axial free-base porphyrin that is operative in these arrays as represented in eq 1.

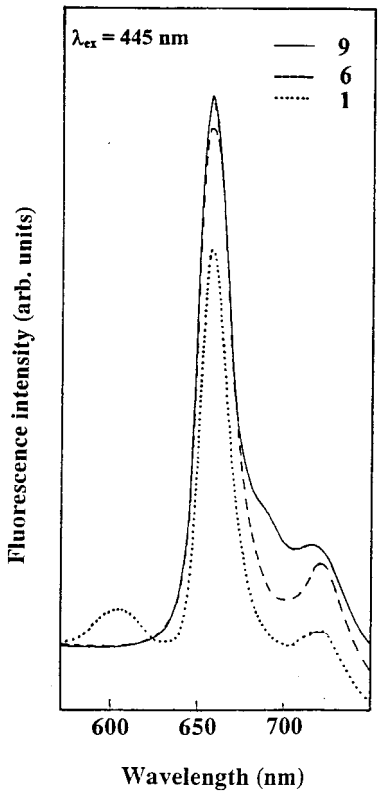

Figure 7. Fluorescence spectra of the trimer **1**, hexamer **6**, and nonamer **9** in CH_2Cl_2 (λ_{ex} = 445 nm).

In this equation, Sn^{IV}P and H_2P are the tin(IV) and free-base porphyrin components present on the two arrays, respectively,

(60) Nimri, S.; Keinan, E. *J. Am. Chem. Soc.* **1999**, *121*, 8978.
(61) $Q_1 = (\phi([(TTP)Sn^{IV}(OH)_2]) - \phi(\text{array}))/\phi([(TTP)Sn^{IV}(OH)_2])$.
(62) Note that the absorbance due to the free-base components of these arrays is a minimum (<5%) at 445 nm. Moreover, the intensities of the fluorescence bands at 656 nm are different for different arrays (equiabsorbing) despite the fact that the free-base to tin(IV) porphyrin ratio is the same in each case (i.e., 2:1).

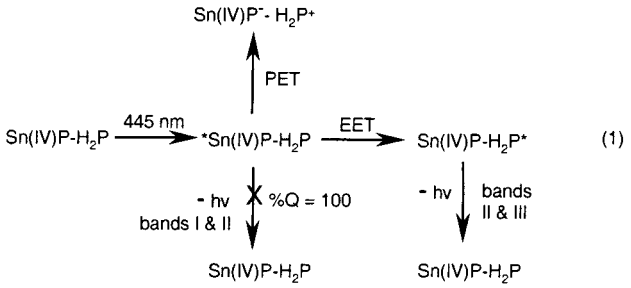

and the asterisk represents the electronically excited singlet state. Such an intramolecular EET is a thermodynamically favored process in these arrays; the singlet-state energy of the tin(IV) porphyrin is higher (2.04 eV) than that of the free-base analogue (1.94 eV) in both **6** and **9**. Additionally, there is a considerable overlap of absorption by the free-base porphyrin and emission by the tin(IV) porphyrin in the 580−640 nm region.[63] Further support for the intramolecular energy transfer being the quenching mechanism comes from the excitation spectral measurements. Overlap of the normalized excitation spectra (emission collected at 720 nm, where the emission is exclusively due to the free-base porphyrin) with the corresponding absorption spectra revealed that the efficiency of the intramolecular EET from the basal tin(IV) porphyrin to the axial free-base porphyrins is ∼85 ± 10% for both **6** and **9**. On the other hand, the corresponding EET efficiency for the lower homologue **1** is only 68 ± 10%.[64] The more efficient EET observed for the higher homologues compared to the trimer in this class of axial-bonding-type hybrid arrays is still unclear. However, we note that the number of acceptors (free-base porphyrins) in the neighborhood of a given donor (tin(IV) porphyrin) increases as one moves from the lower homologue to the higher donor−acceptor ensembles. Thus, unlike the case with the trimer **1**, where EET is from the basal tin(IV) porphyrin to its (own) two axial free-base acceptors, additional energy transfer from a given tin(IV) porphyrin to the free bases ligated at the neighboring tin(IV) centers (i.e., "*trans*-axial" energy transfer) is likely to occur in the higher arrays, leading to more efficient quenching. Interestingly, the high efficiency of energy transfer from the basal tin(IV) porphyrin to the axial free-base acceptors observed here for the axial-bonding-type donor−acceptor arrays **6** and **9** is in contrast with an inefficient flow of energy from a zinc(II) porphyrin to the axially ligated free-base porphyrin, both of which are a part of an elegantly assembled "wheel-and-spoke" array reported by Lindsey and co-workers.[31]

As the quenching efficiency is 100% but the EET efficiency is ∼85% for these arrays, it was found necessary to examine pathways other than the EET to explain the observed quantitative quenching. Among the various other mechanisms considered by us, a photoinduced electron transfer (PET) from the ground-state free-base porphyrin to the singlet-state tin(IV) porphyrin seems to be more probable. This PET reaction leads to a charge-transfer state of the type $Sn^{IV}P^{-}-H_2P^{+}$ (eq 1) and involves free-

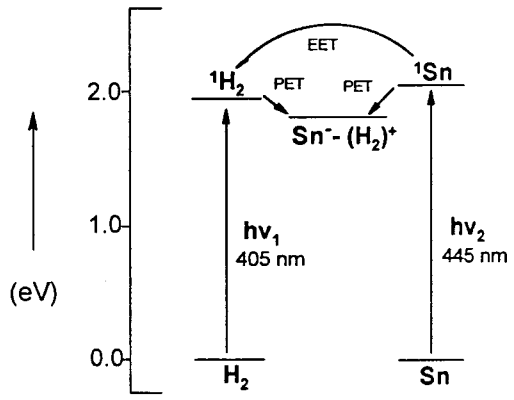

Figure 8. A generalized energy level diagram illustrating the singlet-state dynamics of arrays **6** and **9**. The various energy levels were obtained by the absorption, emission, and redox data. (EET = excitation energy transfer, and PET = photoinduced electron transfer.)

energy changes (ΔG_1(PET) of −0.21 ± 0.04 and −0.25 ± 0.04 eV for **6** and **9**, respectively (eq 2).

$$\Delta G_1(\mathrm{PET}) = E^{\mathrm{ox}}(\mathrm{H_2P}) - E^{\mathrm{red}}(\mathrm{Sn^{IV}P}) - E_{0-0}(\mathrm{Sn^{IV}P}) \qquad (2)$$

$E^{\mathrm{ox}}(H_2P)$ and $E^{\mathrm{red}}(Sn^{IV}P)$ are the oxidation potential of the axial free-base porphyrin and the reduction potential of the basal tin(IV) porphyrin, respectively, and $E_{0-0}(Sn^{IV}P)$ is the singlet-state energy of the tin(IV) porphyrin. We believe that the co-occurrence of strong EET and less prominent PET reactions as illustrated in eq 1 can rationalize the 100% quenching observed for the fluorescence due to the tin(IV) porphyrins of these arrays.

2. Excitation at 405 nm. Excitation of hexane, CH_2Cl_2, or DMF solutions containing **6** or **9** at 405 nm resulted in a typical two-banded fluorescence spectrum, with emission maxima appearing at ∼656 (band II) and ∼718 (band III) nm in each case. The quantum yields of fluorescence as measured in the band III region of **6** and **9** were found to be much lower than those due to monomer **2a** or dimer **4**/trimer **7**.[65] The %*Q* values (%Q_2)[66] for these higher arrays vary between 88 and 97 and are marginally higher than the corresponding values for the trimeric homologue (see Table 2). As noted above, the singlet state of the free-base porphyrin lies at a lower energy than that of the tin(IV) derivative in these arrays, and hence, an EET from the axial free-base porphyrins to the basal tin(IV) porphyrins can be safely ruled out as a quenching mechanism. On the other hand, a PET from the singlet state of the axial free-base porphyrins to the tin(IV) macrocycle seems to be a probable pathway of the observed quenching (see eq 3).

$$\mathrm{Sn^{(IV)}P-H_2P} \xrightarrow{405\ \mathrm{nm}} \mathrm{Sn^{(IV)}P-{}^{*}H_2P} \xrightarrow{\mathrm{PET}} \mathrm{Sn^{(IV)}P^{-}-H_2P^{+}} \qquad (3)$$

Indeed, the free-energy change for this PET (ΔG_2(PET)) is exoergic by 0.11 ± 0.03 and 0.15 ± 0.03 eV for **6** and **9**, respectively (eq 4).

$E_{0-0}(H_2P)$ is the singlet-state energy of the free-base porphyrin. This interpretation is consistent with the similar interpretation made earlier for the trimer **1**.

$$\Delta G_2(\mathrm{PET}) = E^{\mathrm{ox}}(\mathrm{H_2P}) - E^{\mathrm{red}}(\mathrm{Sn^{IV}P}) - E_{0-0}(\mathrm{H_2P}) \qquad (4)$$

(63) Estimation of the Forster overlap integral, J_{Forster}, by utilizing the emission spectrum of $[(TTP)Sn^{IV}(OH)_2]$ and absorption spectrum of H_2TTP gave a value of $(1.40 \pm 0.2) \times 10^{-14}$ cm^6 mmol^{-1}.

(64) Interestingly, the higher fluorescence intensities observed for **6** and **9** compared to that for **1**, under similar sets of experimental conditions (see Figure 7), are consistent with this variation of EET efficiency.

(65) Quantum yields based on the uncorrected fluorescence intensities of the band III region of these spectra were evaluated in comparison with that of H_2TPP. The spectra were deconvoluted for this purpose.

(66) $Q_2 = (\phi(\mathbf{2a}) - \phi(\mathrm{array}))/\phi(\mathbf{2a})$.

Overall, the above analysis reveals that the singlet-state dynamics of these higher arrays involves (i) EET from the basal tin(IV) porphyrin to the axial free-base porphyrin and PET from the ground-state free-base porphyrin to the singlet state of the tin(IV) porphyrin (excitation of the tin(IV) porphyrin) and (ii) PET from the singlet-state free-base porphyrin to the tin(IV) porphyrin (excitation of the free-base porphyrin), as illustrated in Figure 8. While it was possible to experimentally verify the occurrence of an EET reaction, PET has only been inferred on the basis of the thermodynamic arguments.

In summary, new higher order arrays **6** and **9** have been synthesized by adapting a hybrid "organic−inorganic" protocol that involves synthetic manipulation at both the peripheral and axial sites of tin(IV) porphyrin scaffolds. These arrays are highly soluble in various organic solvents and do not aggregate in solution as revealed by their spectral data. The structural features as probed, mainly, by the NMR method indicate a unique axial-bonding-type architectural identity for these systems. While the ground-state properties of both **6** and **9** are close to those of the corresponding reference compounds, the singlet-state properties of these arrays are quite different from those of the monomers constituting them. The fluorescence quenching observed for the tin(IV) and free-base porphyrin components of these bichromophoric systems has been rationalized in terms of intraarray electron- and energy-transfer reactions.

Acknowledgment. Financial support received for this work from CSIR and DST (New Delhi) is gratefully acknowledged. L.G. thanks the UGC for a research fellowship. We gratefully acknowledge the kind help received from Nick Bampos, Eugene Schultz, and Jeremy Sanders (Cambridge, U.K.) in recording the 500 MHz NMR and MALDI-TOF spectra.

Supporting Information Available: UV−vis and ^{1}H NMR spectra of the dimer **5** and trimers **7** and **8**. This material is available free of charge via the Internet at http://pubs.acs.org.

IC010179U